CrossMark
click for updates

Subspace-constrained deconvolution of auditory evoked potentials

Angel de la Torre,[1,a] (iD) Joaquin T. Valderrama,[2,b] (iD) Jose C. Segura,[1,a] (iD) Isaac M. Alvarez,[1,a] (iD) and Jesus Garcia-Miranda[3] (iD)

[1]*Department of Signal Theory, Telematics, and Communications, University of Granada, Granada, Spain*

[2]*National Acoustic Laboratories, Sydney, Australia*

[3]*Department of Algebra, University of Granada, Granada, Spain*

ABSTRACT:

Auditory evoked potentials can be estimated by synchronous averaging when the responses to the individual stimuli are not overlapped. However, when the response duration exceeds the inter-stimulus interval, a deconvolution procedure is necessary to obtain the transient response. The iterative randomized stimulation and averaging and the equivalent randomized stimulation with least squares deconvolution have been proven to be flexible and efficient methods for deconvolving the evoked potentials, with minimum restrictions in the design of stimulation sequences. Recently, a latency-dependent filtering and down-sampling (LDFDS) methodology was proposed for optimal filtering and dimensionality reduction, which is particularly useful when the evoked potentials involve the complete auditory pathway response (i.e., from the cochlea to the auditory cortex). In this case, the number of samples required to accurately represent the evoked potentials can be reduced from several thousand (with conventional sampling) to around 120. In this article, we propose to perform the deconvolution in the reduced representation space defined by LDFDS and present the mathematical foundation of the subspace-constrained deconvolution. Under the assumption that the evoked response is appropriately represented in the reduced representation space, the proposed deconvolution provides an optimal least squares estimation of the evoked response. Additionally, the dimensionality reduction provides a substantial reduction of the computational cost associated with the deconvolution. MATLAB/Octave code implementing the proposed procedures is included as supplementary material.
© 2022 Acoustical Society of America. https://doi.org/10.1121/10.0011423

I. INTRODUCTION

Auditory evoked potentials (AEPs) are useful for the study of the auditory system in the context of hearing research as well as in the context of clinical practice and diagnosis (Burkard and Don, 2007). AEP recording usually includes the repetition of stimuli and the averaging of the responses to improve the signal-to-noise ratio (SNR), usually too low for an isolated response due to the small amplitude of the evoked potentials and the presence of noise (Thornton, 2007).

When stimuli are presented in a repetitive sequence, the standard way for obtaining the response from the electroencephalogram (EEG) is by synchronous averaging of the available epochs (Thornton, 2007). However, synchronous averaging implies a restriction: the inter-stimulus interval (ISI) must be longer than the response duration to avoid overlapping of sequential responses. For this reason, the recording filters and the response length are conventionally configured according to the AEP components to be

recorded: for example, auditory brainstem response (ABR) is recorded in the 100–3000 Hz band with a response duration of around 10 ms; middle latency response (MLR) in the 10–300 Hz band with a response duration of 100 ms; and cortical auditory evoked potentials (CAEPs) in the 1–30 Hz band with a response duration of 1 s (Hall, 2007).

Recording AEPs at a high stimulation rate as well as the simultaneous recording of the responses from different portions of the auditory pathway are relevant for both clinical and research purposes, since they allow the study of neural adaptation mechanisms (Gillespie and Müller, 2009; Thornton and Coleman, 1975; Thornton and Slaven, 1993; Valderrama *et al.*, 2014c) or analysis of the response to complex stimuli more natural than repetitive sequences of clicks (de la Torre *et al.*, 2020; Holt and Ozdamar, 2016; Kohl *et al.*, 2019; Maddox and Lee, 2018; Martinez *et al.*, 2021; Valderrama *et al.*, 2019). However, if the ISI is shorter than the response duration, a deconvolution-based estimation of the AEPs (instead of synchronous averaging) is necessary to disentangle the overlapping responses (Bohórquez and Özdamar, 2006; Eysholdt and Schreiner, 1982; Valderrama *et al.*, 2014b).

There are different deconvolution-based methods proposed in the literature for recovering AEP responses: maximum length sequences (MLS) (Eysholdt and Schreiner, 1982;

[a]Also at: Research Centre for Information and Communications Technologies (CITIC-UGR), University of Granada, Granada, Spain.

[b]Also at: Department of Linguistics, Macquarie University, Sydney, Australia. Electronic mail: joaquin.valderrama@nal.gov.au, joaquin.valderrama@mq.edu.au

Thornton and Slaven, 1993), adjacent-responses (ADJAR) (Woldorff, 1993), quasi-periodic sequence deconvolution (QSD) (Jewett et al., 2004), continuous loop averaging deconvolution (CLAD) (Bohórquez and Özdamar, 2006; Özdamar and Bohórquez, 2006), linear deconvolution for baseline correction (LDBC) (Lütkenhöner, 2010), randomized stimulation and averaging (RSA) (Valderrama et al., 2012), iterative randomized stimulation and averaging (IRSA) (de la Torre et al., 2019; Valderrama et al., 2014b; Valderrama et al., 2016), and randomized stimulation with least squares deconvolution (RSLSD) (Bardy et al., 2014a; Bardy et al., 2014b; Bardy et al., 2014c; de la Torre et al., 2019). Among them, IRSA and RSLSD are particularly attractive because of the flexibility they provide for the stimulus design. While some methods require very specific stimulation sequences (like MLS) or a periodical repetition of a pseudo-random stimulation sequence (like CLAD), the IRSA and RSLSD deconvolutions only require the autocorrelation matrix of the stimulation sequence to be invertible (situation usually verified in most practical situations) (Bardy et al., 2014a; Bardy et al., 2014c; de la Torre et al., 2019; Valderrama et al., 2014c; Valderrama et al., 2016). This less restrictive characteristic of IRSA and RSLSD provides not only more flexibility in the experimental design of audiological tests, but also the possibility of designing audiological experiments with more ecologically valid stimuli (Burkard et al., 2018; de la Torre et al., 2019; Finneran et al., 2019; Martinez et al., 2021; Valderrama et al., 2014c; Valderrama et al., 2016; Valderrama et al., 2019).

In a previous study (de la Torre et al., 2019), we demonstrated that the iterative IRSA procedure converges to the RSLSD solution (which supports the mathematical equivalence of IRSA and RSLSD methods), and we proposed a matrix-based implementation of this algorithm providing an efficient computation of the deconvolution of the AEP responses.

More recently, we proposed the application of a latency-dependent filtering and down-sampling (LDFDS) to the AEP responses (de la Torre et al., 2020). This procedure provides an optimal filtering to the evoked responses and also a substantial reduction of the dimensionality required for representing them. LDFDS was reported to be particularly useful for processing the complete auditory pathway response, i.e., including brainstem, middle latency, and cortical responses simultaneously. The underlying idea with LDFDS is that each portion of the evoked response involves a specific frequency bandwidth, and therefore an optimal filtering (and also an optimal down-sampling) should change dynamically with the latency, with wider bandwidth and higher sampling rate at early latency (i.e., in the region of ABR), which progressively decrease as the latency increases (i.e., for the MLR and CAEP components). In this previous article, we demonstrated that LDFDS provides a significant noise reduction thanks to the latency-dependent filtering. Additionally, thanks to the latency-dependent down-sampling, the complete auditory pathway response (including ABR, MLR, and CAEP), usually requiring more than 10 000 samples at a constant sampling rate, can be correctly represented after LDFDS with only 40 samples per decade (a

decade is the interval between a latency T and a latency $10 \cdot T$), i.e., with around 120 samples. Therefore, the evoked response can be represented in the original signal representation or, equivalently, in a reduced representation, requiring a significantly smaller number of samples (or components) in this last case.

While LDFDS was applied after the deconvolution in our previous work (de la Torre et al., 2020), in the current work, we propose to perform the deconvolution (either with IRSA or with RSLSD) in the reduced representation given by LDFDS, i.e., we propose a deconvolution constrained to the subspace defined by LDFDS. This proposal implies two important differences. On one hand, as we discuss in the present work, the subspace-constrained deconvolution provides an optimal least squares estimation of the evoked response. On the other hand, since the IRSA algorithm involves iterative matrix products and RSLSD involves a matrix division, a substantial reduction of the problem dimensionality (typically from several thousand to around 100 or 200 dimensions) implies a substantial reduction of the computational cost in both deconvolution algorithms.

In this work, we present the mathematical foundation of the LDFDS-based subspace-constrained least squares (SC-LS) deconvolution as an optimal solution when the evoked response is assumed to be contained in the associated subspace (i.e., properly represented with LDFDS). We also discuss the quality of the proposed estimation (in terms of the expected energy of the estimation error) as well as the computational cost. The experimental results, including both simulations and estimation of real AEP responses, illustrate the utility of the proposed subspace-constrained deconvolution for recording AEPs, including the response of the complete auditory pathway.

II. SUBSPACE-CONSTRAINED DECONVOLUTION

A. Least squares deconvolution

In an AEP recording procedure, the EEG is usually modeled as a convolutional process (Jewett et al., 2004; Özdamar and Bohórquez, 2006),

$$y(n) = s(n) * x(n) + n_0(n), \qquad (1)$$

where $y(n)$, $s(n)$, and $n_0(n)$ are digital signals representing, respectively, the EEG, the stimulation sequence (consisting of one impulse at the beginning of each stimulation event), and the noise affecting the EEG; n is the index for the samples ($n \in \{0, ..., N-1\}$, where N is the number of samples of the EEG); $x(n)$ represents the response evoked by each stimulus [with $x(n)$ null for $n > (J-1)$, J being the length of the evoked response]; and the asterisk (*) represents discrete time convolution.

This convolutional model can be rewritten using a matrix notation (de la Torre et al., 2019),

$$\mathbf{y} = S\mathbf{x} + \mathbf{n}_0, \qquad (2)$$

where $\mathbf{y}$, $S\mathbf{x}$, and $\mathbf{n}_0$ are N-component column vectors (representing the EEG signal, the convolution of the stimulation signal with the response, and the noise, respectively), $\mathbf{x}$ is a J-component column vector representing the evoked response, and S is a $(N \times J)$ matrix (with N rows and J columns) with $S(n,j) = s(n-j)$ providing the convolution $s(n) * x(n)$ as a matrix operation.

The deconvolution of $\mathbf{y}$, i.e., the estimation of the response $\mathbf{x}$, can be formulated either as an over-determined system of linear equations (with N equations and J unknowns, being $N \gg J$), in the context of linear algebra, or as a multiple linear regression problem, in the context of statistics (Gentle, 1998; Goldberger et al., 1964; Hayashi, 2000; Lawson and Hanson, 1974). Assuming linearity and uncorrelated stationary white noise (i.e., if linearity, exogeneity, and homocedasticity conditions are verified), the ordinary least squares (LS) solution provides a minimum-variance unbiased estimation of the response (Hayashi, 2000). The LS criterion minimizes the sum of the squared residuals or equivalently the squared distance between the EEG and the expected convolution,

$$\hat{\mathbf{x}}_{LS} = \arg\min_{\mathbf{x}} ||\mathbf{y} - S\mathbf{x}||^2, \tag{3}$$

and the solution derived from this criterion, i.e., the LS deconvolution, is (Gentle, 1998; Hayashi, 2000; Press et al., 2002)

$$\hat{\mathbf{x}}_{LS} = (S^T S)^{-1} S^T \mathbf{y}, \tag{4}$$

where S^T is the transpose of S.

By defining the matrix S_k as the normalized and transposed form of S (i.e., $S_k = S^T/K$, where K is the number of impulses in the stimulation sequence) and taking into account that $R_s = S_k S$ is the normalized $(J \times J)$ autocorrelation matrix of the stimulation sequence $s(n)$, the LS deconvolution can be rewritten as

$$\hat{\mathbf{x}}_{LS} = R_s^{-1} S_k \mathbf{y} = R_s^{-1} \mathbf{z}_0, \tag{5}$$

where $\mathbf{z}_0 = S_k \mathbf{y}$ is a J-component vector obtained as the synchronous averaging of the EEG. The derivation of the LS estimation is detailed in Sec. 1 of the supplementary material.[1]

The LS estimation of the evoked response requires the synchronous averaging of the EEG ($\mathbf{z}_0$) and the inversion of the $(J \times J)$ normalized autocorrelation matrix of the stimulation sequence (R_s^{-1}). This LS estimation can be obtained by matrix division [as proposed in RSLSD (Bardy et al., 2014a; Bardy et al., 2014b; Bardy et al., 2014c)]. Alternatively, the IRSA procedure (de la Torre et al., 2019) proposes an iterative LS estimation of the response according to the following recursion:

$$\hat{\mathbf{x}}_i = \hat{\mathbf{x}}_{i-1} + \alpha \mathbf{z}_{i-1}, \tag{6}$$

$$\mathbf{z}_i = \mathbf{z}_0 - R_s \hat{\mathbf{x}}_i, \tag{7}$$

where α is a convergence parameter that must be small enough ($\alpha < 2/\max \lambda_i$, λ_i being the eigenvalues of R_s) to guarantee the stability of the algorithm.

B. LDFDS

Since each portion of the evoked response requires a specific bandwidth (range 100–3000 Hz for ABR; 10–300 Hz for MLR; 1–30 Hz for CAEPs), a latency-dependent filtering was proposed by de la Torre et al. (2020) for optimally filtering the AEP responses. The latency-dependent filtering is implemented as a matrix operator, where the impulsive response changes from row to row, to adapt to the bandwidth required at each latency (lower cut-off frequency as the latency increases). Moreover, since the bandwidth changes with the latency, according to the sampling theorem, the sampling rate can also be adapted to optimal values at each specific latency. The latency-dependent down-sampling can easily be implemented by appropriately selecting specific rows of the latency-dependent filtering matrix.

This way, the LDFDS is implemented by means of a $(J_r \times J)$ matrix V_r, with J being the dimensionality of the representation space of the original AEP response and J_r that of the reduced representation space (i.e., after the filtering and down-sampling). The reduced representation (with J_r components) of the LS deconvolution is obtained by multiplying the LDFDS matrix V_r and the J-component original vector $\hat{\mathbf{x}}_{LS}$ (representing the LS estimation of the AEP response),

$$(\hat{\mathbf{x}}_{LS})_r = V_r \hat{\mathbf{x}}_{LS}. \tag{8}$$

With the proposed procedure, the noise out of the frequency bands of interest is efficiently removed, and the dimensionality is reduced typically from several thousand samples to 40 samples per decade (around 120 samples for accurately representing the complete auditory pathway response). Additionally, the rows of the LDFDS matrix are orthonormalized, which preserves the metrics (i.e., the distances and energies) in the reduced representation space. The orthonormality of the rows allows the recovery of the optimally latency-dependent filtered response in the original representation (at the original sampling rate and with J components), $\hat{\mathbf{x}}_{ldf}$, by multiplying the reduced representation and the transpose of the LDFDS matrix,

$$\hat{\mathbf{x}}_{ldf} = V_r^T (\hat{\mathbf{x}}_{LS})_r. \tag{9}$$

C. SC-LS deconvolution

If we assume that the response to be estimated $\mathbf{x}$ is appropriately represented with the reduced representation $\mathbf{x}_r$ given by V_r (or, equivalently, if the latency-dependent filtering provided by V_r is appropriate for the evoked response $\mathbf{x}$), then we can write

$$\mathbf{x} = \mathbf{x}_{ldf} = V_r^T \mathbf{x}_r, \tag{10}$$

and the convolutional model provided in Eq. (2) can be rewritten as

J. Acoust. Soc. Am. **151** (6), June 2022

de la Torre et al. 3747

$$\mathbf{y} = S V_r^T \mathbf{x}_r + \mathbf{n}_0. \tag{11}$$

This equation is mathematically similar to Eq. (2), with the following differences: (i) the unknown is the J_r-component vector $\mathbf{x}_r$ instead of the J-component vector $\mathbf{x}$, and (ii) it involves the $(N \times J_r)$ matrix $(S V_r^T)$ instead of the $(N \times J)$ matrix S. Equation (11) can again be formulated as another over-determined system of linear equations, or as a multiple linear regression problem, with the difference of the significant dimensionality reduction provided by LDFDS. This dimensionality reduction implies that the convolution problem is constrained to the subspace associated with the matrix V_r, or equivalently, the solution of the system of equations is forced to be in the subspace of responses compatible with the latency-dependent filtering, with J_r freedom degrees (instead of J). The formal LS solution is similar to that in Eq. (4), but using $(S V_r^T)$ instead of S,

$$
\begin{aligned}
\hat{\mathbf{x}}_{rLS} &= \left((S V_r^T)^T (S V_r^T) \right)^{-1} (S V_r^T)^T \mathbf{y} \\
&= \left(V_r S^T S V_r^T \right)^{-1} V_r S^T \mathbf{y} \\
&= \left(V_r R_s V_r^T \right)^{-1} V_r S_k \mathbf{y} \\
&= \left(V_r R_s V_r^T \right)^{-1} V_r \mathbf{z}_0 = R_{sr}^{-1} \mathbf{z}_{0r},
\end{aligned} \tag{12}
$$

where R_{sr} and $\mathbf{z}_{0r}$ are, respectively, R_s and $\mathbf{z}_0$ projected into the subspace. According to this equation, the subspace-constrained LS deconvolution of the EEG can be obtained with the following steps: (i) the autocorrelation matrix R_s and the synchronous averaging of the EEG $\mathbf{z}_0$ must be transformed to the subspace using the transformation V_r; (ii) the autocorrelation matrix in the reduced representation must be inverted; and (iii) the inverted reduced autocorrelation matrix must be applied to the reduced synchronous averaging. As can be observed, the LS deconvolution in Eq. (12) is similar to that in Eq. (5), with the difference that the problem is solved in the reduced representation space.

Since it is assumed that the LS solution is contained in the subspace defined by V_r, this procedure requires that the evoked response is correctly described in this subspace. Otherwise, the procedure will provide a biased solution, as discussed in Sec. 2 of the supplementary material.[1]

Interestingly, since the matrix to be inverted has a size $(J_r \times J_r)$ instead of $(J \times J)$, the subspace-constrained deconvolution provides a substantial reduction of the computational load. Moreover, since the solution is expected to be contained in the subspace, the subspace constrain and the LS criterion guarantee that the $\hat{\mathbf{x}}_{rLS}$ solution is closer to the evoked response $\mathbf{x}$ than the non-constrained solution $\hat{\mathbf{x}}_{LS}$.

As in the case of the original representation space, the subspace-constrained LS deconvolution can be implemented with matrix division as proposed for RSLSD. Alternatively, it can be implemented with the IRSA recursion constrained to the subspace, i.e., using R_{sr} and $\mathbf{z}_{0r}$ instead of R_s and $\mathbf{z}_0$ in Eqs. (6) and (7),

$$\hat{\mathbf{x}}_{ir} = \hat{\mathbf{x}}_{i-1r} + \alpha \mathbf{z}_{i-1r}, \tag{13}$$

$$\mathbf{z}_{ir} = \mathbf{z}_{0r} - R_{sr} \hat{\mathbf{x}}_{ir}, \tag{14}$$

and the demonstration of the IRSA convergence to the LS solution is similar in both the original and the reduced representation space.

D. Energy of the error in the estimated response

Taking into account Eqs. (2) and (5), we can write

$$
\begin{aligned}
\hat{\mathbf{x}}_{LS} &= R_s^{-1} S_k \mathbf{y} = R_s^{-1} S_k (S \mathbf{x} - \mathbf{n}_0) \\
&= R_s^{-1} R_s \mathbf{x} + R_s^{-1} S_k \mathbf{n}_0 \\
&= \mathbf{x} + R_s^{-1} S_k \mathbf{n}_0,
\end{aligned} \tag{15}
$$

and the error of the LS estimation is

$$\mathbf{e}_{LS} = \hat{\mathbf{x}}_{LS} - \mathbf{x} = R_s^{-1} S_k \mathbf{n}_0 = R_s^{-1} \mathbf{n}_A, \tag{16}$$

where $\mathbf{n}_A = S_k \mathbf{n}_0$ is the synchronous averaging of the noise affecting the EEG. The noise affecting the EEG is unknown, and therefore the error affecting the estimated evoked potential cannot be calculated. However, taking into account the statistics of the noise (described with its covariance matrix Σ_{n_0}) and the previous equation, we can calculate the covariance matrix $\Sigma_{e_{LS}}$ of the error affecting the estimated response (whose trace is the expected energy of the error),

$$\Sigma_{e_{LS}} = R_s^{-1} S_k \Sigma_{n_0} S_k^T (R_s^{-1})^T = R_s^{-1} \Sigma_{n_A} R_s^{-1}, \tag{17}$$

where Σ_{n_A} is the $(J \times J)$ covariance matrix of the noise after the synchronous averaging (which is a positive semidefinite, Toeplitz, and symmetric matrix, as Σ_{n_0}), and the fact that R_s (as well as its inverse) is symmetric has also been taken into account.

A similar derivation can be done when the LS deconvolution is performed in the reduced representation space. In such case, the error affecting the LS estimation in the reduced representation space is

$$\mathbf{e}_{rLS} = \hat{\mathbf{x}}_{rLS} - \mathbf{x}_r = (V_r R_s V_r^T)^{-1} V_r \mathbf{n}_A, \tag{18}$$

and the corresponding covariance matrix is

$$\Sigma_{e_{rLS}} = (V_r R_s V_r^T)^{-1} V_r \Sigma_{n_A} V_r^T (V_r R_s V_r^T)^{-1}, \tag{19}$$

where both the reduced autocorrelation matrix $(V_r R_s V_r^T)$ and its inverse are symmetric.

The LS criterion guarantees that the LS solution is optimal (in the sense that it provides an unbiased and minimum-variance estimation of $\mathbf{x}_r$ under the required assumptions), and therefore, if the response is expected to be contained in the subspace defined by V_r, the energy of the error (as well as the variance of the estimation) is expected to be smaller when the LS solution is constrained to this subspace. Under the LS assumptions (including uncorrelated and stationary white noise), it is easy to demonstrate that the energy of the error decreases or, equivalently, that the trace of the covariance matrix of the error decreases,

3748   J. Acoust. Soc. Am. **151** (6), June 2022

de la Torre et al.

$$\mathrm{tr}(\Sigma_{e_{rLS}}) < \mathrm{tr}(\Sigma_{e_{LS}}). \tag{20}$$

The demonstration is included in Sec. 3 of the supplementary materials.[1]

E. Comparison of subspace-constrained deconvolution vs LDFDS after deconvolution

The LS criterion guarantees that $\hat{\mathbf{x}}_{rLS}$ is an optimal solution under several assumptions: $\mathbf{x}$ is in the subspace, $s(n)$ and $n_0(n)$ are uncorrelated, and $n_0(n)$ is stationary white noise. We have verified that the energy of the expected error for $\hat{\mathbf{x}}_{rLS}$ is less than or equal to that for $\hat{\mathbf{x}}_{LS}$. However, when LDFDS was proposed, $\hat{\mathbf{x}}_{LS}$ was first estimated and then projected into the subspace,

$$(\hat{\mathbf{x}}_{LS})_r = V_r \hat{\mathbf{x}}_{LS} = V_r R_s^{-1} \mathbf{z}_0, \tag{21}$$

and it was demonstrated to be effective for noise reduction [i.e., $(\hat{\mathbf{x}}_{LS})_r$ substantially improves $\hat{\mathbf{x}}_{LS}$]. Therefore, one could wonder whether the subspace-constrained deconvolution $\hat{\mathbf{x}}_{rLS}$ proposed here improves or not the estimation obtained when LDFDS is applied after a non-constrained deconvolution $(\hat{\mathbf{x}}_{LS})_r$, previously proposed in de la Torre et al. (2020).

Of course, under the required assumptions, the LS criterion guarantees that the subspace-constrained deconvolution is better, but some analysis is also interesting. Both approaches can be compared taking into account the trace of the covariance matrix of the error affecting the corresponding estimations. The covariance matrix of the error is given in Eq. (19) for $\hat{\mathbf{x}}_{rLS}$. In the case of $(\hat{\mathbf{x}}_{LS})_r$, the covariance matrix of the error is

$$\Sigma_{(e_{LS})_r} = V_r R_s^{-1} \Sigma_{nA} R_s^{-1} V_r^T. \tag{22}$$

In Sec. 4 of the supplementary material,[1] the traces of both covariance matrices are compared. As expected, under the assumptions (particularly, in the case of white noise), it is demonstrated that the trace for the subspace-constrained deconvolution is less than or equal to that for $(\hat{\mathbf{x}}_{LS})_r$,

$$\mathrm{tr}(\Sigma_{e_{rLS}}) \leq \mathrm{tr}(\Sigma_{(e_{LS})_r}). \tag{23}$$

Interestingly, the equality occurs if $R_s = I$. This situation never takes place in a deconvolution problem (because if $R_s = I$, then the optimal solution is obtained with the synchronous averaging). However, R_s is usually relatively close to the identity matrix, and therefore the solutions $(\hat{\mathbf{x}}_{LS})_r$ and $\hat{\mathbf{x}}_{rLS}$ are expected to be close.

III. EXPERIMENTS AND RESULTS

The experiments have been designed to compare (i) the LS solution, (ii) the LS solution transformed to the reduced subspace, and (iii) the subspace-constrained LS solution, corresponding to the estimations $\hat{\mathbf{x}}_{LS}$, $(\hat{\mathbf{x}}_{LS})_r$, and $\hat{\mathbf{x}}_{rLS}$, and referred to as LS, LS-R, and SC-LS, respectively. These are compared in terms of both the quality of the estimated

responses and the computational cost of the procedures. According to the RSLSD and IRSA procedures, we have compared implementations based on both matrix division (LS$_{\mathrm{MD}}$, LS-R$_{\mathrm{MD}}$, and SC-LS$_{\mathrm{MD}}$) and iterative estimation (LS$_{\mathrm{It}}$, LS-R$_{\mathrm{It}}$, and SC-LS$_{\mathrm{It}}$).

The quality evaluation of the estimated responses requires an *a priori* knowledge of the clean signal, to be used as reference, which is not possible with real AEP responses (because the estimations are always affected by some residual noise). Therefore, the quality evaluations are based on simulations (where a noisy EEG can be synthesized using a known clean AEP response, which can be used as reference). The evaluation of the computational cost is based on real EEG signals.

A. Experimental design

For the experiments involving real EEG signals, the stimulation consisted in rarefaction clicks of 0.1 ms at 74 dB normal hearing level (nHL) presented at different average stimulation rates, between 1.39 and 44.44 stimuli per second (stim/sec). The 0 dB nHL reference level was estimated as described in Martinez et al. (2022), i.e., as the mean threshold level estimated in a sample of 10 normal-hearing adults (five female, 23–38 years) who presented pure-tone threshold levels within the normal range in the 0.5–8 kHz frequency range and had no history of any type of auditory dysfunction. At each average stimulation rate, the ISI has a uniform distribution within one octave of variation (e.g., 480–960 ms for average stimulation rate of 1.39 stim/s; 240–480 ms for 2.78 stim/s; etc.). Six stimulation conditions are considered, with one octave of variation from condition to condition (i.e., double average stimulation rate and half ISI-limits for the next condition). The EEGs were recorded with surface electrodes located at the forehead (active), right mastoid (reference), and middle forehead (ground) using a preamplifier with 70 dB gain and 1–3500 Hz bandwidth (Valderrama et al., 2013; Valderrama et al., 2014a; Valderrama et al., 2014c). The preamplified EEG signal was digitized (44 100 Hz, 16 bits/sample), low-pass filtered (4000 Hz cut-off frequency), and down-sampled to 14 700 Hz. Eye-blinking artifacts were suppressed with the iterative template matching and suppression algorithm (ITMS) (Valderrama et al., 2018). The EEG database [previously used in de la Torre et al. (2020)] contains recordings from eight subjects (aged 26–58 years, one female) with six ISI conditions for each subject and 684 s of EEG recording for each ISI condition. All the participants of this database met the inclusion criteria of reporting no hearing difficulties and absence of a history of auditory dysfunction. To obtain the response of the complete auditory pathway, the AEP response extends from 0 to 1000 ms, i.e., the response length is $J = 14\,700$ samples. The LDFDS is performed with a resolution of 40 samples/decade, which provides a response length in the reduced representation space of $J_r = 117$ samples.

The experiments involving simulations are designed with a configuration similar to that of the real experiments

J. Acoust. Soc. Am. **151** (6), June 2022

de la Torre *et al.*   3749

(same ISI conditions and EEG duration). The grand-average AEP responses obtained in de la Torre *et al.* (2020) at each ISI condition were used as reference clean AEP responses to synthesize the simulated EEGs. These reference AEP responses were latency-dependent filtered with a resolution of 40 samples/decade. The EEGs are synthesized according to the convolutional model in Eq. (1). The noise contaminating the EEGs was bandpass random noise (with flat spectral density in the range [1.5–800] Hz and ±20 dB/decade slope out of the passband). It was prepared from white Gaussian noise, filtered with a first-order 1.5–800 Hz Butterworth bandpass filter. The noise level was adjusted to obtain a final SNR (after the standard LS deconvolution) around +10 dB, which is a reasonable SNR for typical AEP estimations (de la Torre *et al.*, 2020).

In the simulation-based experiments, the AEP response $\hat{\mathbf{x}}$ is estimated from the EEG $\mathbf{y}$ either with the LS, LS-R, or SC-LS procedures. Using the clean reference $\mathbf{x}$, the error can be estimated as $\mathbf{e} = \hat{\mathbf{x}} - \mathbf{x}$, and the different procedures can easily be compared in terms of the error energy. However, since the noise affecting the EEG is a random process, the error energy estimations are strongly affected by statistical fluctuations. For this reason, the three procedures have been compared in terms of the expected error energy (statistically consistent with the measured error energies but more stable than them) using the trace of the covariance matrix of the respective errors in Eqs. (17), (22), and (19) for LS, LS-R, and SC-LS, respectively. The simulations have been repeated 100 times for each ISI condition, and expected error measurements have been averaged.

For the experiments involving real EEGs and evaluation of the computational cost, the LS, LS-R, and SC-LS estimations have been obtained with algorithms based on both RSLSD (i.e., involving matrix division) and IRSA (i.e., involving iterative estimation). MATLAB/Octave functions implementing the RSLSD and IRSA algorithms for LS, LS-R, and SC-LS estimations are described in Sec. 5 of the supplementary materials,[1] together with a demonstration script providing a simulation and examples of use of these functions. The convergence criterion for the iterative estimations was set either to 290 dB (more accurate) or to 120 dB (faster). The computational cost was evaluated in terms of execution time, measured using a desktop computer with an Intel-Core i7–3770 central processing unit (CPU), 3.40 GHz, 8.00 GB RAM running the algorithms with MATLAB.

B. Quality of the LS, LS-R, and SC-LS estimations

Figure 1 represents an example of the AEP responses obtained in the simulations for one of the 100 repetitions. The figure includes the clean AEP responses used for the EEG synthesis (and as reference for the quality estimations) and the different estimations based on LS, LS-R, and SC-LS (with the matrix division implementation). The six responses in each panel correspond to the different ISI conditions considered in the simulations, from 480–960 ms (top) to 15–30 ms (bottom). The latency axis is logarithmically

scaled to appropriately represent the response of the complete auditory pathway, from the ABRs to the cortical responses. The main waves of the AEP response are labeled, and the stimulation artifact can be observed within the first ms. As can be observed, the LS estimation is strongly affected by noise (due to the noise added to the EEG). The LS-R and SC-LS estimations are significantly less affected by noise. Interestingly, the LS-R and SC-LS estimations are very similar. The comparison of the different estimations is detailed in Sec. 6.1 of the supplementary material.[1]

The quality of each estimation has been evaluated using the expected SNR, defined as the ratio of the signal energy to the expected error energy, expressed in dB, where the expected error energy was estimated as the trace of the covariance matrix of the residual error,

$$\text{SNR}_{\text{dB}} = 10 \log_{10}\left(\frac{E(\mathbf{x})}{E(\mathbf{e})}\right) \approx 10 \log_{10}\left(\frac{E(\mathbf{x})}{\text{tr}(\Sigma_e)}\right). \quad (24)$$

The supplementary material[1] includes, in Sec. 6.2, a description of the autocorrelation functions of the noise and the averaged noise (providing Σ_{n_0} and Σ_{n_A}, respectively) and the main diagonal of the covariance matrix of the residual error for the LS, LS-R, and SC-LS estimations.

Table I shows the expected SNR obtained for the LS, LS-R, and SC-LS estimations, based on the respective covariance matrices. The table includes means and standard deviation (SD) for each ISI condition. As can be observed (and consistent with the example in Fig. 1), there is a substantial improvement in LS-R and SC-LS with respect to LS (associated with the latency-dependent filtering) and a very slight improvement of SC-LS with respect to LS-R (associated with the LS resolution constrained to the subspace). Table II evaluates the improvement of LS-R with respect to LS and that of SC-LS with respect to LS-R, including the mean and SD of the SNR difference and the p value of a paired Student's t-test (i.e., the probability of the null hypothesis of statistical independence). The improvement associated with the latency-dependent filtering is between 6.3 and 13.8 dB, depending on the ISI condition, which is consistent with the results reported in de la Torre *et al.* (2020). The subspace-constrained deconvolution provides a moderate (but systematic) improvement, between 0.006 and 0.043 dB, depending on the ISI condition. These improvements are statistically significant, as can be appreciated from the p values in Table II.

The supplementary material[1] includes, in Sec. 6.3, results of the SNRs estimated from the error observed at each repetition of the simulation. The SNRs obtained from the expected error and from the observed error are statistically consistent (same mean values) even though the SDs are much greater for the SNRs derived from the observed error (due to statistical fluctuations).

C. Computational cost of the procedures

The computational cost of the deconvolution procedures is compared in Table III. The three deconvolution procedures (LS, LS-R, SC-LS) have been implemented with

3750   J. Acoust. Soc. Am. **151** (6), June 2022
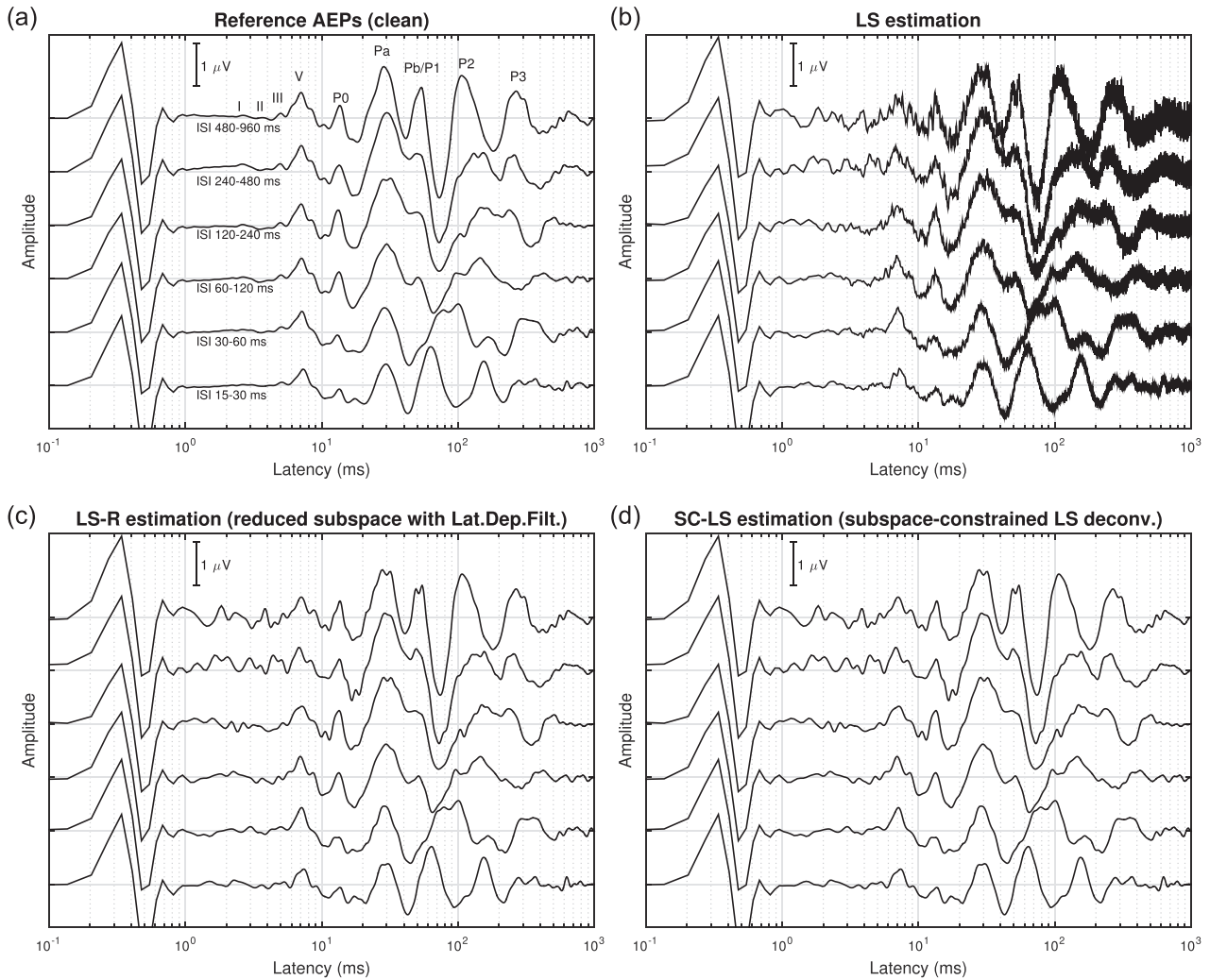
de la Torre *et al.*

FIG. 1. AEP responses obtained in the simulations for one repetition. The different panels represent (a) the template responses used as reference, (b) the LS estimations (obtained in the original representation space), (c) the LS-R estimations (obtained by applying dimensionality reduction based on the LDFDS to the LS estimations), and (d) the SC-LS estimations (subspace-constrained LS deconvolution). The plots in each panel correspond to the AEP responses at each ISI condition.

matrix division (using the RSLSD algorithm) and with the iterative estimation (using the IRSA algorithm with convergence criterion of either 290 or 120 dB). The table includes the execution time for each ISI condition (average execution time per subject). The last row represents the execution time for the complete test (including the six ISI conditions). The

TABLE I. SNR mean [standard deviation (SD) in parenthesis] in dB for the LS, LS-R, and SC-LS estimations, obtained in simulations with 100 repetitions for each ISI condition. The SNR measurements are based on the covariance matrix of the error.

ISI condition	LS mean (SD) (dB)	LS-R mean (SD) (dB)	SC-LS mean (SD) (dB)
480–960 ms	9.351 (0.002)	23.181 (0.014)	23.188 (0.014)
240–480 ms	9.252 (0.012)	22.672 (0.023)	22.686 (0.023)
120–240 ms	9.589 (0.008)	21.778 (0.035)	21.810 (0.035)
60–120 ms	7.614 (0.004)	17.645 (0.041)	17.688 (0.041)
30–60 ms	11.472 (0.008)	19.180 (0.045)	19.209 (0.045)
15–30 ms	11.610 (0.008)	17.928 (0.030)	17.948 (0.030)
Average	9.815 (1.379)	20.397 (2.238)	20.421 (2.230)

results for LS and LS-R (with similar execution times) reveal that the computational cost of the latency-dependent filtering is very small compared with that of the deconvolution. However, the SC-LS provides a significant reduction of the execution time with respect to LS or LS-R, thanks to the dimensionality reduction (from $J = 14\,700$ to $J_r = 117$). While the IRSA procedure provides a relevant computational cost reduction with respect to RSLSD in the case of LS and LS-R, when the deconvolution is constrained to the subspace the computational costs are very similar. Section 7.1 of the supplementary material[1] provides more details about the execution times (including initialization and time devoted to each iteration). It also provides a comparison of the execution times measured with a faster computer.

The execution times reported in Table III correspond to a response length of 14 700 samples. To evaluate the influence of the response length over the computational cost, the execution time has been evaluated for J ranging between 14 700 (1000 ms) and 147 (10 ms). Figure 2 represents the total execution time per subject as a function of the response length, for the LS-R and SC-LS deconvolution algorithms

TABLE II. SNR improvement provided by LS-R with respect to LS and by SC-LS with respect to LS-R, in dB, obtained in simulations with 100 repetitions for each ISI condition. The SNR measurements are based on the trace of the covariance matrix of the error. The table includes mean, SD, and the p parameter for a paired Student's t-test.

| | LS-R vs LS | | SC-LS vs LS-R | |
ISI condition	Mean (SD) (dB)	p	Mean (SD) (dB)	p
480–960 ms	13.830 (0.013)	1.4×10^{-300}	0.006 (4.4×10^{-4})	4.0×10^{-117}
240–480 ms	13.419 (0.018)	2.0×10^{-287}	0.014 (8.1×10^{-4})	3.8×10^{-124}
120–240 ms	12.188 (0.038)	6.1×10^{-250}	0.033 (1.1×10^{-3})	1.2×10^{-149}
60–120 ms	10.031 (0.037)	2.1×10^{-242}	0.043 (4.9×10^{-4})	6.2×10^{-194}
30–60 ms	7.708 (0.040)	9.2×10^{-228}	0.028 (5.6×10^{-4})	4.5×10^{-171}
15–30 ms	6.318 (0.023)	2.7×10^{-244}	0.020 (4.2×10^{-4})	4.0×10^{-168}
Average	10.582 (2.830)	$<1 \times 10^{-320}$	0.024 (0.012)	7.5×10^{-211}

(LS has not been included in the plot, since it provides execution times similar to those of LS-R). As can be observed, the execution time decreases with the response length, and the improvements are less important as J decreases (because the ratio J/J_r decreases with J).

D. Responses provided by the SC-LS deconvolution

Figure 3 represents the grand-average of the AEP responses provided by the SC-LS deconvolution. These responses correspond to the solutions provided by the SC-LS$_{MD}$ algorithm (i.e., SC-LS criterion implemented with matrix division). As in Fig. 1, the latency axis is logarithmically scaled to represent the responses of the different portions of the auditory pathway. This responses are very similar to those obtained in de la Torre et al. (2020) and represented in Fig. 1(a), because they have been obtained from the same EEG database and also because the solutions provided by LS-R (i.e., applying the latency-dependent filtering) and SC-LS are very similar (the energy of the difference between both solutions is about 31 dB below the signal energy in these experiments). Section 7.2 of the supplementary material[1] evaluates the differences among the solutions provided by the different deconvolution algorithms considered in this paper.

E. Grand-average and individual AEP responses

Figure 4 shows, in the top-left panel, the grand-average AEP responses across participants obtained with SC-LS$_{MD}$

at different stimulation rates. The rest of the panels show the individual responses for each participant. The AEP components are labeled in the grand-average response presented at the top (corresponding to ISI 480–960 ms). The latency has been limited in these plots to the range [1–1000] ms to ease the analysis of the evoked response (detailed individual responses including also the stimulation artifact portion can be found in Sec. 7.3 of the supplementary material[1]).

The plots with individual traces (subjects 1–8) visually show that all the AEP components from wave I of the ABR to the P3 can be identified in all subjects at the slow presentation rate. Overall, the amplitude of the components decreases as the stimulus rate increases. Moreover, the grand-average AEP responses presented in Fig. 4 (top left), and the individual subplots show that the components from wave I to Pa are highly reproducible and that they can be tracked from the slow to the faster presentation rates. However, the P1/Pb, P2, and P3 components present a higher variability as rate increases, and they are more difficult to track from the slow to the faster rates.

In addition, subject 7 presents a post-auricular muscle response (PAMR) in all the AEP traces (an action potential occurring at approximately 13 ms after the stimulus onset resulting from the contraction of a muscle located behind the ear, i.e., the post-auricular muscle). The amplitude of the PAMR decreases as the stimulus rate increases. A remarkable negative peak at the latency corresponding to N1 (between Pb/P1 and P2) is also observed for this subject at

TABLE III. Mean execution time across subjects for different ISI conditions in the experiments with real EEGs. The columns correspond to the different deconvolution algorithms. The rows correspond to the different ISI conditions. The last row represents the execution time for processing the six ISI conditions.

| ISI (ms)	LS$_{MD}$ (RSLSD) (s)	LS$_{It}$ (IRSA-290dB) (s)	LS$_{It}$ (IRSA-120dB) (s)	LS-R$_{MD}$ (RSLSD) (s)	LS-R$_{It}$ (IRSA-290dB) (s)	LS-R$_{It}$ (IRSA-120dB) (s)	SC-LS$_{MD}$ (RSLSD) (s)	SC-LS$_{It}$ (IRSA-290dB) (s)	SC-LS$_{It}$ (IRSA-120dB) (s)
480–960	20.23	0.63	0.55	20.50	0.61	0.53	0.59	0.59	0.59
240–480	20.91	1.79	1.09	20.74	1.75	1.09	1.01	1.03	1.02
120–240	21.58	3.75	2.03	21.34	3.71	2.01	1.74	1.77	1.75
60–120	22.10	7.05	3.60	22.18	6.99	3.65	2.47	2.52	2.49
30–60	22.99	13.48	6.66	22.99	13.47	6.63	3.52	3.65	3.59
15–30	25.87	17.16	13.05	25.82	17.00	12.97	6.31	6.42	6.32
All	**133.69**	**43.86**	**26.98**	**133.58**	**43.53**	**26.88**	**15.63**	**15.98**	**15.76**
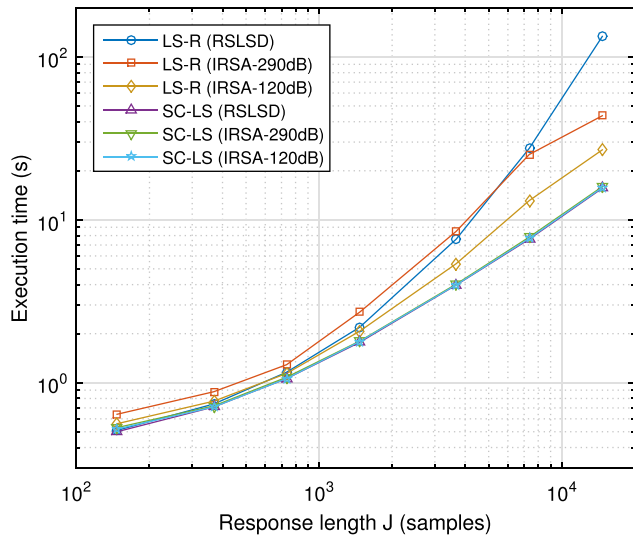
FIG. 2. (Color online) Mean execution time across subjects required by the different algorithms for processing all the ISI conditions, as a function of the response length J.

slow presentation rates. Section 7.3 of the supplementary material[1] includes a comparison of the grand-average responses including and excluding this particular subject (when subject 7 is excluded, the morphology of the grand-average responses is quite similar, except for the amplitude reduction in waves P0 and N1).

IV. DISCUSSION AND CONCLUSIONS

In this work, we propose the subspace-constrained LS deconvolution for the estimation of the AEPs, based on the LDFDS dimensionality reduction. This work presents the mathematical foundation of the subspace-constrained deconvolution, a theoretical analysis of the residual error (including a demonstration of the error reduction with respect to the conventional LS deconvolution and with respect to LS-R, i.e., when the LDFDS is applied after the LS
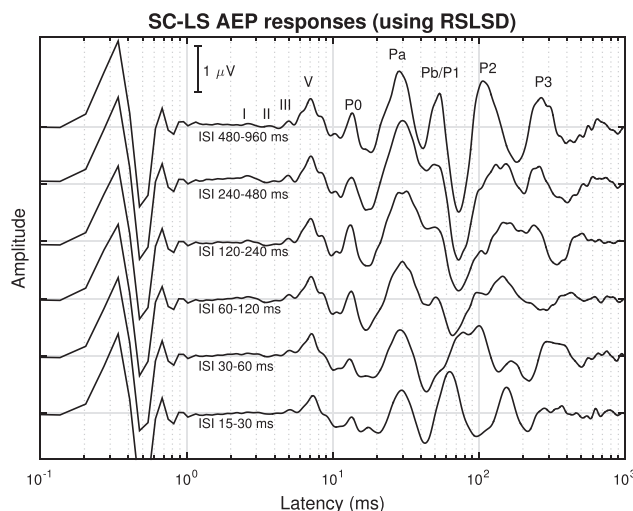

FIG. 3. Grand-average responses obtained with $SC\text{-}LS_{MD}$ for the experiments using real EEG signals.

deconvolution), and experimental evaluation of the improvement provided by the proposed method in terms of quality of the estimated AEP responses and computational cost.

Regarding the quality of the estimations, SC-LS significantly improves the LS solution (thanks to the noise removal provided by the latency-dependent filtering). Even though the LS criterion guarantees (under the LS assumptions) that the SC-LS solution is also better than or equal to the LS-R solution, the improvement is moderate in this case (the difference between both solutions is about 31 dB below the response energy, i.e., usually masked by the residual noise), probably because the autocorrelation matrix of the stimulation sequence R_s is close to the identity matrix. Therefore, in practice, the solutions provided by SC-LS and LS-R are very similar.

A relevant difference between SC-LS and LS-R is the requirement that the response in the convolutional model **x** belongs to the subspace. In the case of LS-R, if **x** is not correctly represented in the subspace (for example, if the response is truncated to remove the stimulation artifact), the estimated response does not contain components out of the subspace, but the subspace component is not biased. However, in the case of SC-LS, if **x** is not correctly represented in the subspace, the subspace component is biased (due to the transference of energy from the orthogonal complement to the reduced subspace). This effect would be a disadvantage of the proposed method if the reduced representation space was not appropriate to represent the signal involved in the convolution. For this reason, in SC-LS, an appropriate design of the reduced subspace is critical to appropriately represent the signal involved in the convolution (including both the biological response and the stimulation artifact if it was present).

The dimensionality reduction provided by LDFDS (from $J = 14\,700$ to $J_r = 117$ in the reported experiments) provides several practical advantages for the subspace-constrained deconvolution. The most evident is the reduction of the computational cost associated with the deconvolution, with a reduction of the execution time by a factor of 8.5 in the case of the RSLSD algorithm (from 133.7 to 15.6 s) and a factor 1.7 in the case of IRSA-120dB (from 27.0 to 15.8 s). Additionally, the dimensionality reduction would allow the analysis of the matrix to be inverted [for example, an analysis of its eigenvalues is useful for the estimation of the matrix condition number (Bardy *et al.*, 2014b)], easier as the size of the matrix decreases. Finally, the potential problems associated with matrix inversion (due to low eigenvalues or high condition number of the matrix to be inverted) are alleviated in the reduced representation because the condition number of the matrix to be inverted decreases according to the Cauchy interlacing theorem (the LS deconvolution is better conditioned in the reduced representation space).

In conventional LS deconvolution, the computational cost of IRSA is significantly smaller than that of RSLSD. This advantage disappears when the deconvolution is
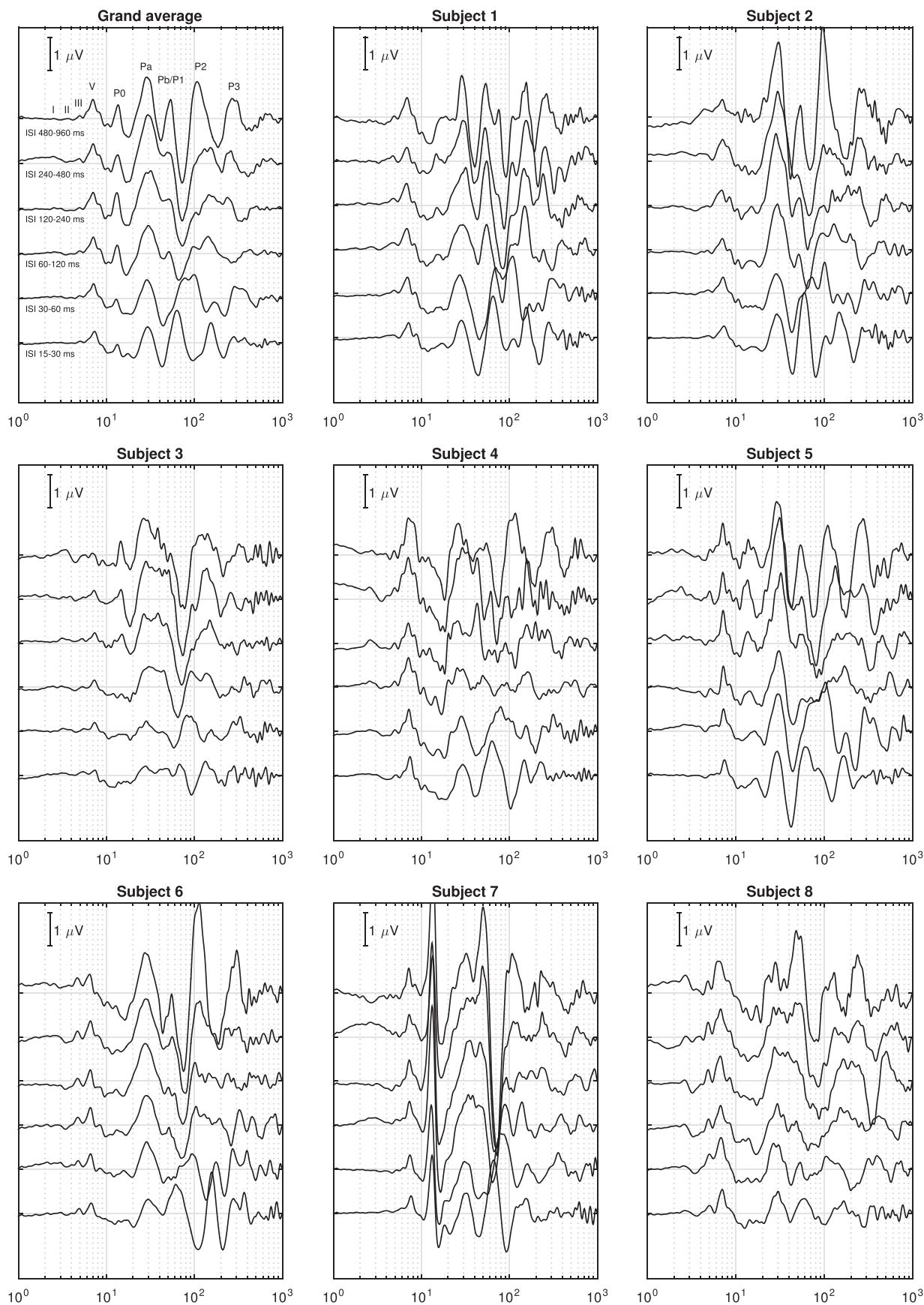
FIG. 4. Grand-average and individual AEP responses obtained with the SC-LS$_{MD}$ algorithm at different stimulation rates. The AEP components are labeled in the grand-average response at ISI 480–960 ms. The horizontal and vertical axes correspond, respectively, to latency (in ms) and amplitude. The latency axis has been limited to the range [1–1000] ms.

constrained to the subspace. Two factors contribute to reduce the advantage of IRSA: on one hand, the matrix to be inverted in the subspace is not Toeplitz, and therefore a fast-Fourier-transform-based matrix product is not possible in the reduced representation. On the other hand, part of the advantage of IRSA with respect to RSLSD was associated with the high dimensionality of the matrix to be inverted and vanishes as the dimensionality decreases. As a consequence, the RSLSD implementation of SC-LS (with a simpler formulation and directly providing the solution at convergence) has a computational cost similar to that of IRSA.

The SC-LS deconvolution of overlapping AEPs described in this paper along with the representation of the deconvolved AEPs in the logarithmic time scale enables the comprehensive and uninterrupted visualization of all the AEP components of the auditory pathway (from the cochlea to the cortex). While this type of AEP representation is currently non-standard, we believe that it provides a change of paradigm with potential to become the natural way in which AEPs are represented (both in clinical and research applications) due to the important advantages that it provides relative to the traditional representation of AEPs (in which the ABR, MLR, or CAEP components can be only separately visualised). For example, the proposed comprehensive AEP representation would facilitate the exploration of peripheral and central interactions resulting from both bottom-up and top-down processes (Asilador and Llano, 2021; Lesicko and Llano, 2017) or as a possible diagnostic tool for auditory neuropathy spectrum disorder [as this population is characterized by presenting clear cortical but absent brainstem components (Hood, 2007)].

The amplitude reduction observed in the PAMR in subject 7 as the stimulus rate increased is consistent with the results obtained by Zakaria et al. (2019), the only study that to the best of our knowledge has investigated the influence of the stimulus rate on the morphology of the PAMR. Zakaria et al. (2019) evaluated three stimulus repetition rates, 6.1, 11.1, and 17.1 stim/s, and found that the PAMR threshold increased for the faster repetition rate. In the present study, we show that the PAMR can be reliably recorded at stimulation rates up to 44.4 stim/s (i.e., ISI 15–30 ms). Future research aimed at characterizing the morphology of the PAMR at faster rates shall benefit from deconvolution algorithms, such as the proposed SC-LS.

At group level, the grand-average AEPs and the individual responses show that peripheral components of the response (i.e., from wave I to Pa) can be visually tracked down from the slow to the faster stimulus rates. In contrast, the tracking of central components, such as the P1/Pb, P2, and P3, as stimulus rate increases is not straightforward, particularly for ISIs lower than 60–120 ms. Tracking AEP components from a control scenario (in which the neural generators are known) to novel exploratory scenarios (in which the morphology of the responses has not been documented) is an efficient strategy to identify the neural generators of those components (Elberling and Don, 2007). For

example, this strategy could be applied to identify AEP components resulting from the analysis of transient AEP responses from binaural stimuli (Martinez et al., 2021) or from ecologically valid stimuli such as natural speech (Valderrama et al., 2019). The difficulty in tracking central components in the present study could be the result of a sub-optimal placement of the active electrode on the head (situated in Fz in this study), as the P1-P2 complex maximizes its magnitude in Cz (Bardy et al., 2014b) and the P3 component in CPz (Hall, 2007). Placing the active electrode far from the neural generator sites may have led to an inefficient characterization of central AEP components, adding an extra difficulty to track these components as a function of the stimulus presentation rate. In this respect, future studies investigating the morphology of both peripheral and central AEP components at different rates shall benefit from the use of a multi-channel EEG recording setup.

Furthermore, the analysis of the individual AEP waveforms has revealed the existence of the P3 component in all the participants at the slow stimulus rate. This finding was contrary to our expectations, since the P3 component is associated with novelty and expectation and is typically evoked by stimuli presented at slow rates (e.g., 1 or 0.5 stim/s) via the oddball paradigm [by comparing the morphology from AEP responses elicited by a deviant stimulus relative to a frequent stimulus (Hall, 2007; Sharma, 2021)]. In contrast, the present study uses sequences of a single stimulus (clicks) in which the maximum ISI doubles the minimum ISI. It could be the case that this broad distribution of the ISI induces some degree of novelty on the participant, thus evoking either (i) a consistent P3 component in all the responses of the stimulus sequence or (ii) a large P3 component only in those responses in which the degree of novelty is higher (probably those with longer ISIs). To respond to this question, a multi-response deconvolution approach would be required to carry out a time-invariant analysis, similar to the one proposed by Valderrama et al. (2016).

A potential limitation of the proposed deconvolution method (affecting any deconvolution procedure, also when it is performed in the complete representation space) is the linearity requirement for the least squares criterion. The convolutional method described in Eq. (1) [or its matrix formulation described in Eq. (2)] assumes that the auditory system is linear and time invariant (LTI). However, it is well known that auditory evoked responses do not have a linear behavior with the stimulation level [there is a threshold effect, a non-linear growing with the stimulation level, and a saturation effect (Hall, 2007)] and are not time invariant [the responses change with the state of the auditory system (Valderrama et al., 2016)]. A possible strategy to deal with this limitation consists in the formulation of a multi-response deconvolution with different possible responses associated with different stimulation levels [as proposed in Martinez et al. (2022)] or with different states of the auditory system [as proposed in Valderrama et al. (2016)]. This way, under a multi-response formulation of the deconvolution, the

non-LTI auditory system can be modeled as an LTI-like system. The multi-response deconvolution, necessary for exploring the response of the complete auditory pathway using complex stimulation patterns, would increase the computational requirements dramatically (a preliminary analysis suggests to us that the computational cost would increase with the square of the number of responses considered in the multi-response model). Under this new paradigm, the computational optimization proposed in this article is expected to be very relevant.

In summary, the subspace-constrained deconvolution together with the dimensionality reduction provided by LDFDS provide a substantial quality improvement with respect to the conventional LS solution (and very slight improvement with respect to LS-R, this improvement not being very useful in practice) and provide a substantial computational cost reduction with respect to LS or LS-R, particularly important for the estimation of the complete auditory pathway response. The reduction of both the execution time and the dimensionality, together with the inherent flexibility of IRSA or RSLSD, provide new perspectives in the design of evoked potential experiments, with more ecological stimuli, involving the simultaneous deconvolution of multiple responses (associated with multiple categories of acoustical events) and including the response of the complete auditory pathway (Martinez *et al.*, 2021; Valderrama *et al.*, 2019).

ACKNOWLEDGMENTS

[1]See the supplementary material at https://www.scitation.org/doi/suppl/10.1121/10.0011423 for a PDF file presenting the derivation of the least squares solution for an over-determined system of linear equations (Sec. 1); a description of the effect of an inappropriate subspace selection (Sec. 2); the mathematical demonstration of the noise reduction provided by the subspace-constrained LS estimation (Sec. 3); a comparison of subspace-constrained deconvolution vs LDFDS after deconvolution (Sec. 4); MATLAB/Octave functions implementing the LS, LS-R, and SC-LS procedures (Sec. 5); additional experiments with simulations (Sec. 6); and additional experiments with real EEGs (Sec. 6). A compressed directory with examples and MATLAB/Octave scripts and functions, aiming to help the reader apply the subspace-constrained LS deconvolution procedure described in this paper, is also included.

Asilador, A., and Llano, D. A. (**2021**). "Top-down inference in the auditory system: Potential roles for corticofugal projections," Front. Neural Circuits **14**, 615259.

Bardy, F., Dillon, H., and Dun, B. V. (**2014a**). "Least-squares deconvolution of evoked potentials and sequence optimization for multiple stimuli under low-jitter conditions," Clin. Neurophysiol. **125**, 727–737.

Bardy, F., Dun, B. V., Dillon, H., and Cowan, R. (**2014b**). "Least-squares (LS) deconvolution of a series of overlapping cortical auditory evoked potentials: A simulation and experimental study," J. Neural Eng. **11**, 046016.

Bardy, F., Dun, B. V., Dillon, H., and McMahon, C. M. (**2014c**). "Deconvolution of overlapping cortical auditory evoked potentials recorded using short stimulus onset-asynchrony ranges," Clin. Neurophysiol. **125**, 814–826.

Bohórquez, J., and Özdamar, Ö. (**2006**). "Signal to noise ratio analysis of maximum length sequence deconvolution of overlapping evoked potentials," J. Acoust. Soc. Am. **119**, 2881–2888.

Burkard, R. F., and Don, M. (**2007**). "The auditory brainstem response," in *Auditory Evoked Potentials: Basic Principles and Clinical Application*, edited by R. Burkard, M. Don, and J. Eggermont (Lippincott Williams & Wilkins, Baltimore, MD), pp. 229–253.

Burkard, R. F., Finneran, J. J., and Mulsow, J. (**2018**). "Comparison of maximum length sequence and randomized stimulation and averaging methods on the bottlenose dolphin auditory brainstem response," J. Acoust. Soc. Am. **144**, 308–318.

de la Torre, A., Valderrama, J. T., Segura, J. C., and Alvarez, I. M. (**2019**). "Matrix-based formulation of the iterative randomized stimulation and averaging method for recording evoked potentials," J. Acoust. Soc. Am. **146**, 4545–4556.

de la Torre, A., Valderrama, J. T., Segura, J. C., and Alvarez, I. M. (**2020**). "Latency-dependent filtering and compact representation of the complete auditory pathway response," J. Acoust. Soc. Am. **148**, 599–613.

Elberling, C., and Don, M. (**2007**). "Detecting and assessing synchronous neural activity in the temporal domain (snr, response detection)," in *Auditory Evoked Potentials: Basic Principles and Clinical Application*, edited by R. Burkard, M. Don, and J. Eggermont (Lippincott Williams & Wilkins, Baltimore, MD), pp. 102–123.

Eysholdt, U., and Schreiner, C. (**1982**). "Maximum length sequences: A fast method for measuring brain-stem-evoked responses," Int. J. Audiol. **21**, 242–250.

Finneran, J. J., Mulsow, J., and Burkard, R. F. (**2019**). "Signal-to-noise ratio of auditory brainstem responses (ABRs) across click rate in the bottlenose dolphin (*Tursiops truncatus*)," J. Acoust. Soc. Am. **145**, 1143–1151.

Gentle, J. E. (**1998**). *Numerical Linear Algebra for Applications in Statistics* (Springer, New York).

Gillespie, P. G., and Müller, U. (**2009**). "Mechanotransduction by hair cells: Models, molecules, and mechanisms," Cell **139**, 33–44.

Goldberger, A., Shenhart, W., and Wilks, S. (**1964**). "Classical linear regression," in *Econometric Theory* (Wiley, New York).

Hall, J. W. (**2007**). *New Handbook of Auditory Evoked Potentials* (Pearson Education, Boston), pp. 58–108.

Hayashi, F. (**2000**). *Econometrics* (Princeton University, Princeton, NJ).

Holt, F., and Ozdamar, O. (**2016**). "Effects of rate (0.3–40/s) on simultaneously recorded auditory brainstem, middle and late responses using deconvolution," Clin. Neurophysiol. **127**, 1589–1602.

Hood, L. J. (**2007**). "Auditory neuropathy and dys-synchrony," in *Auditory Evoked Potentials: Basic Principles and Clinical Application*, edited by R. Burkard, M. Don, and J. Eggermont (Lippincott Williams & Wilkins, Baltimore, MD), pp. 275–290.

Jewett, D. L., Caplovitz, G., Baird, B., Trumpis, M., Olson, M. P., and Larson-Prior, L. J. (**2004**). "The use of qsd (q-sequence deconvolution) to recover superposed, transient evoked-responses," Clin. Neurophysiol. **115**, 2754–2775.

Kohl, M. C., Schebsdat, E., Schneider, E. N., Niehl, A., Strauss, D. J., Özdamar, Ö., and Bohórquez, J. (**2019**). "Fast acquisition of full-range auditory event-related potentials using an interleaved deconvolution approach," J. Acoust. Soc. Am. **145**, 540–550.

Lawson, C. L., and Hanson, R. J. (**1974**). *Solving Least Squares Problems* (Prentice-Hall, Englewood Cliffs, NJ).

Lesicko, A. M. H., and Llano, D. A. (**2017**). "Impact of peripheral hearing loss on top-down auditory processing," Hear. Res. **343**, 4–13.

Lütkenhöner, B. (**2010**). "Baseline correction of overlapping event-related responses using a linear deconvolution technique," NeuroImage **52**, 86–96.

Maddox, R. K., and Lee, A. K. C. (**2018**). "Auditory brainstem responses to continuous natural speech in human listeners," eNeuro **5**, e0441.

Martinez, M., Valderrama, J. T., Alvarez, I., Vargas, J. L., and de la Torre, A. (**2021**). "The transient response to interaural time differences," in *Proceedings of the XXVII International Evoked Response Audiometry Study Group (IERASG-2021)*, June 14–July 9, p. 50.

Martinez, M., Valderrama, J. T., Alvarez, I., Vargas, J. L., and de la Torre, A. (**2022**). "Auditory brainstem responses obtained with randomised stimulation level," Int. J. Audiol. (published online).

Özdamar, Ö., and Bohórquez, J. (**2006**). "Signal-to-noise ratio and frequency analysis of continuous loop averaging deconvolution (clad) of overlapping evoked potentials," J. Acoust. Soc. Am. **119**, 429–438.

3756   J. Acoust. Soc. Am. **151** (6), June 2022

de la Torre *et al.*

Press, W. H., Teutolsky, S. A., Vetterling, W. T., and Flannery, B. P. (**2002**). *Numerical Recipes in C: The Art of Scientific Computing*, 2nd ed. (Cambridge University, New York).

Sharma, M. (**2021**). "Episode 3: Late-late shows in AEPdom—Beyond obligatory potentials: When just turning on the same stimulus is not enough," in *Basic Concepts of Clinical Electrophysiology in Audiology*, edited by J. Durrant, C. Fowler, J. Ferraro, and S. Purdy (Plural Publishing, San Diego, CA), pp. 336–348.

Thornton, A. R. D. (**2007**). "Instrumentation and recording parameters," in *Auditory Evoked Potentials: Basic Principles and Clinical Application*, edited by R. Burkard, M. Don, and J. Eggermont (Lippincott Williams & Wilkins, Baltimore, MD), pp. 73–101.

Thornton, A. R. D., and Coleman, A. (**1975**). "The adaptation of cochlear and brainstem auditory evoked potentials in humans," Electroencephalogr. Clin. Neurophysiol. **39**, 399–406.

Thornton, A. R. D., and Slaven, A. (**1993**). "Auditory brainstem responses recorded at fast stimulation rates using maximum length sequences," Br. J. Audiol. **27**, 205–210.

Valderrama, J. T., Alvarez, I., de la Torre, A., Segura, J. C., Sainz, M., and Vargas, J. L. (**2012**). "Recording of auditory brainstem response at high stimulation rates using randomized stimulation and averaging," J. Acoust. Soc. Am. **132**, 3856–3865.

Valderrama, J. T., de la Torre, A., Alvarez, I., Segura, J. C., Sainz, M., and Vargas, J. L. (**2013**). "A portable, modular, and low cost auditory brainstem response recording system including an algorithm for automatic identification of responses suitable for hearing screening," in *Proceedings of the IEEE/EMBS Special Topic Conference on Point-of-Care HealthCare Technologies (PoCHT)*, January 16–18, Bangalore, India, pp. 180–189.

Valderrama, J. T., de la Torre, A., Alvarez, I., Segura, J. C., Sainz, M., and Vargas, J. L. (**2014a**). "A flexible and inexpensive high-performance auditory evoked response recording system appropriate for research purposes," Biomed. Tech. **59**, 447–459.

Valderrama, J. T., de la Torre, A., Alvarez, I., Segura, J. C., Thornton, A. R. D., Sainz, M., and Vargas, J. L. (**2014b**). "Auditory brainstem and middle latency responses recorded at fast rates with randomized stimulation," J. Acoust. Soc. Am. **136**, 3233–3248.

Valderrama, J. T., de la Torre, A., Alvarez, I., Segura, J. C., Thornton, A. R. D., Sainz, M., and Vargas, J. L. (**2014c**). "A study of adaptation mechanisms based on abr recorded at high stimulation rate," Clin. Neurophysiol. **125**, 805–813.

Valderrama, J. T., de la Torre, A., and Dun, B. V. (**2018**). "An automatic algorithm for blink-artifact suppression based on iterative template matching: Application to single channel recording of cortical auditory evoked potentials," J. Neural Eng. **15**, 016008.

Valderrama, J. T., de la Torre, A., Dun, B. V., and Segura, J. C. (**2019**). "Towards the recording of brainstem and cortical evoked potentials from the fine structure of natural speech," in *Proceedings of the XXVI International Evoked Response Audiometry Study Group (IERASG) Biennial Symposium*, June 30–July 4, Sydney, Australia.

Valderrama, J. T., de la Torre, A., Medina, C., Segura, J. C., and Thornton, A. R. D. (**2016**). "Selective processing of auditory evoked responses with iterative-randomized stimulation and averaging: A strategy for evaluating the time-invariant assumption," Hear. Res. **333**, 66–76.

Woldorff, M. G. (**1993**). "Distortion of ERP averages due to overlap from temporally adjacent ERPs: Analysis and correction," Psychophysiology **30**, 98–119.

Zakaria, M. N., Abdullah, R., Nik, O., and Nik, A. (**2019**). "The influence of stimulus repetition rate on tone-evoked post-auricular muscle response (PAMR) threshold," Ear Hear. **40**(4), 1039–1042.